quantum beam science

MDPI

Supplementaly Materials

Implementation and Applications of a Precision Weak-Field Sample Environment for Polarized Neutron Reflectometry at J-PARC

Takayasu Hanashima [1,*], Kazuhiro Akutsu-Suyama [1], Yoshimasa Ohe [1], Satoshi Kasai [1], Hiroshi Kira [1], Azusa N. Hattori [2], Ai I. Osaka [2,†], Hidekazu Tanaka [2], Jun-Ichi Suzuki [1] and Kazuhisa Kakurai [3,4]

[1] Neutron Science and Technology Center, Comprehensive Research Organization for Science and Society (CROSS), 162-1 Shirakata, Ibaraki 319-1106, Japan
[2] SANKEN, Osaka University, Mihogaoka 8-1, Ibaraki 567-0047, Japan
[3] Institute of Multidisciplinary Research for Advanced Materials, Tohoku University, 2-1-1 Katahira, Aoba-ku, Sendai 980-8577, Japan
[4] RIKEN Center for Emergent Matter Science (CEMS), Wako 351-0198, Japan
* Correspondence: t_hanashima@cross.or.jp; Tel.: +81-29-219-5300
† Current address: Division of Electrical and Electronic Engineering, University of Hyogo, Himeji 671-2280, Japan.

1. Conventional magnetic field environment (10 kOe magnet at BL17)

A photograph of the conventional 10 kOe electromagnet used at the SHARAKU beamline (BL17) is shown in Figure S1. This system has been widely employed for polarized neutron reflectometry (PNR) experiments requiring strong magnetic fields.

The magnet consists of an iron-core electromagnet with pole pieces arranged to produce a uniform magnetic field across a 50 mm gap, supported by an H-shaped iron yoke that helps suppress stray magnetic fields along the neutron beam axis. An automated sample changer is integrated into the system, allowing up to five samples to be mounted simultaneously with vertical motion capabilities of up to 80 mm.

While this system enables measurements in the field range of approximately −10 to +10 kOe, it exhibits residual magnetization due to the iron cores, limiting its applicability to weak-field experiments. A detailed description of the system's performance characteristics and limitations is provided in Section 2.1 of the main text.

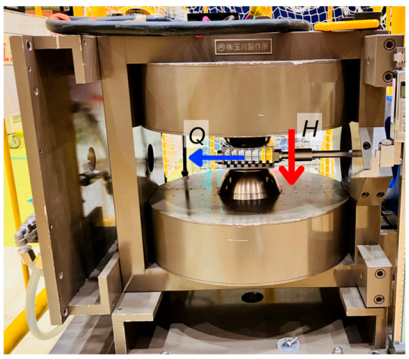


Figure S1. Photograph of the 10 kOe magnet used at BL17. The red arrow indicates the direction of the magnetic field. The brown-painted structure corresponds to the H-shaped iron yoke, within which the iron-core pole pieces and the automated sample changer are housed.

2. Weak-field sample environment (WFSE): vertical (transverse, ⊥ beam) configuration

In this paper, the terms horizontal and vertical configuration are mainly used; these correspond to the longitudinal (∥ beam) and transverse (⊥ beam) geometries that are commonly employed in magnetic scattering studies.

Figure S2 presents the details of the newly developed weak-field sample environment (WFSE). Figure S2(a) shows the calculated magnetic-field distribution when a current of 16.6 A is applied to a pair of Helmholtz coils (HC, each 256 mm × 256 mm × 72 mm), generating a field of 100 Oe at the sample position. Within a region of 60 mm × 60 mm × 60 mm around the sample position, the field inhomogeneity remains below 1.1%. Depending on the experimental requirements, the orientation of the coils can be toggled to change the direction of the magnetic field relative to the neutron beam. Figure S2(b) provides an external schematic of the WFSE centered on the HC, indicating the outer dimensions and the neutron beam direction. By detaching the upper frame that houses the HC from the lower support and reassembling them, the configuration can be switched between vertical and horizontal. Figure S2(c) shows a photograph of the WFSE in the vertical configuration installed at the SHARAKU (BL17) beamline of J-PARC MLF. In the horizontal configuration, the magnetic field is aligned with the beam direction; once magnetic continuity is verified, only a minor adjustment of the beamline polarization is required. In contrast, in the vertical configuration, the field direction differs from that of the beam direction, which can potentially reduce the neutron polarization. To avoid depolarization of the polarized neutrons, the magnetic connection between the beamline and the WFSE in the vertical configuration must provide a sufficiently gradual field transition. Here, the spatial and temporal variations of the magnetic field experienced by polarized neutrons were calculated for a sample field of 50 Oe, within a range of 10 mm along the beam axis (Y-axis) and 40 mm along the field direction (Z-axis). Since typical samples used in PNR experiments have a surface area of about 10 mm × 10 mm, the above range can be regarded as a practical condition. The HC, the WFSE, and the guide coils of the beamline, together with their magnetic fields, are arranged symmetrically around the sample position. To ensure a sufficiently gradual variation of the magnetic field and thereby avoid depolarization of polarized neutrons, the following the adiabaticity condition was applied in the design [1–3]:

$$\omega_L/\omega_B \geq 10 \tag{S1}$$

where ω_L is the Larmor precession frequency of the neutron and ω_B represents the change of the magnetic field experienced by the neutron. Figure S2(d) plots ω_L/ω_B as a function of the distance from the sample position, under the optimized magnetic connection between the WFSE in the vertical configuration and the beamline. Here, Y = 0 and Z = 0 represent polarized neutrons passing through the center of the WFSE. Nonzero Y values values indicate offsets along the beam axis, while nonzero Z values indicate offsets along the field direction (in millimeters). For example, at Y = 5 mm and Z = 20 mm, the minimum value of $\omega_L/\omega_B = 10$ is obtained between 0 mm and 90 mm from the WFSE center. These results demonstrate that polarized neutrons can be preserved in the vertical (transverse, ⊥ beam) configuration.

Figure S2(e) shows the magnetic field at the sample position as a function of the HC current. The relationship can be expressed as

$$H\ (\text{Oe}) = 5.953 \times I\ (\text{A}) + 1.4 \tag{S2}$$

The offset of 1.4 Oe originates from the geomagnetic field and the guide field of the beamline, the latter being oriented perpendicular to the field generated by the HC. As a result, the field at the sample position is tilted from the vertical axis, and the tilt angle increases as the HC current decreases. At zero current, the tilt angle reaches approximately 90°. A slight difference is observed between the vertical and horizontal

configurations, which originates from differences in the experimental setup. In the Supplementary Materials measurements, a different power supply was used for the HC, and the mounting method of the gaussmeter probe was improved to enhance positional stability. These modifications resulted in a small change in the effective calibration values but did not affect the reproducibility or reliability of the WFSE performance. If necessary, a current–field calibration curve can be quickly re-established in the vertical configuration as well.

In summary, these evaluations confirm that the WFSE enables stable application of weak magnetic fields and reliable preservation of polarized neutrons in the vertical configuration, thereby establishing practical conditions for PNR experiments.

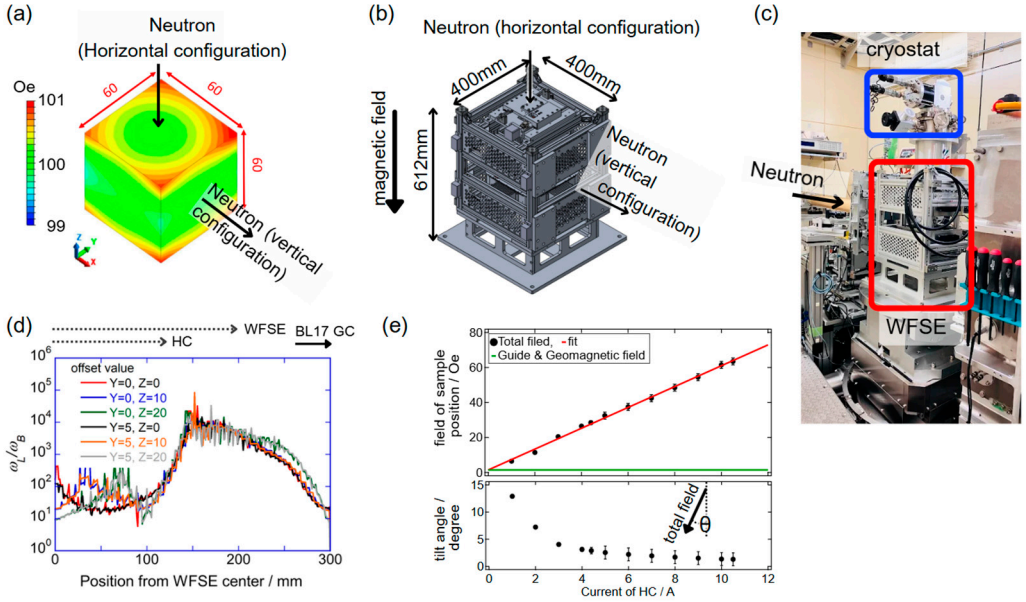


Figure S2. Schematics and installation of the WFSE in the horizontal (longitudinal, ∥ beam) and the vertical (transverse, ⊥ beam) configuration: (a) Calculated magnetic field distribution when 16.6 A is applied to the Helmholtz coil pair (HC), generating 100 Oe at the sample position. (b) Design drawing of the WFSE centered on the HC, showing the outer dimensions and neutron beam direction. (c) Photograph of the WFSE installed at the SHARAKU (BL17) beamline of J-PARC MLF. For comparison, the horizontal configuration aligns the field parallel to the neutron beam axis, while in the vertical configuration the field is applied perpendicular to it. (d) Calculated values of ω_L/ω_B as a function of distance from the WFSE center. The legend indicates the offset values (in mm) of the neutron beam relative to the sample center in the beam (Y) and field (Z) directions. These offsets correspond to an effective beam footprint of approximately 10 mm (Y-axis) × 40 mm (Z-axis), which is typical for PNR experiments. (e) Magnetic field at the sample position as a function of the HC current. The linear fit yields H(Oe) = 5.953 × I(A) + 1.44. The lower panel shows the tilt angle of the field direction relative to the vertical axis, which arises from the influence of the guide and geomagnetic fields.

3. Polarization efficiency correction

This section provides the theoretical framework used to correct the measured spin-dependent reflectivities based on the polarization and flipping efficiencies of the optical

components. For a more general treatment of the formalism, readers are referred to the original literature[4–6]. The derivation presented here complements the summary provided in the main text (Sections 2.1 and 3.1) and requires simultaneous treatment of Eqs. (S3)–(S7), since no single equation alone is sufficient to determine the polarization efficiencies.

At the BL17 beamline, the polarizer is a V-shaped transmission-type device composed of two multilayer mirrors, while the analyzer is a reflection-type multilayer mirror. When both the upstream and downstream spin flippers are inactive, the measured polarization state predominantly corresponds to (−+), and the associated intensity is denoted as $I(00)$.

To extract the true spin-dependent reflectivities $\hat{R}$, the measured intensities must be corrected using the following optical parameters:

P_1: polarization efficiency of the upstream polarizer
A_2: polarization efficiency of the downstream analyzer
F_1: flipping efficiency of the upstream flipper
F_2: flipping efficiency of the downstream flipper

These corrections are represented by the following matrix equation:

$$\hat{I} = \hat{F}_1\hat{F}_2\hat{P}_1\hat{A}_2\hat{R},$$

$$\hat{I} = \begin{pmatrix} I(00) \\ I(01) \\ I(10) \\ I(11) \end{pmatrix}, \hat{R} = \begin{pmatrix} R^{-+} \\ R^{--} \\ R^{++} \\ R^{+-} \end{pmatrix}, \hat{F}_1 = \begin{pmatrix} 1 & 0 & 0 & 0 \\ 0 & 1 & 0 & 0 \\ 1-F_1 & 0 & F_1 & 0 \\ 0 & 1-F_1 & 0 & F_1 \end{pmatrix}, \hat{F}_2 = \begin{pmatrix} 1 & 0 & 0 & 0 \\ 1-F_2 & F_2 & 0 & 0 \\ 0 & 0 & 1 & 0 \\ 0 & 0 & 1-F_2 & F_2 \end{pmatrix}$$

$$\hat{P}_1 = \begin{pmatrix} (1+P_1)/2 & 0 & (1-P_1)/2 & 0 \\ 0 & (1+P_1)/2 & 0 & (1-P_1)/2 \\ (1-P_1)/2 & 0 & (1+P_1)/2 & 0 \\ 0 & (1-P_1)/2 & 0 & (1+P_1)/2 \end{pmatrix} \quad \text{(S3)}$$

$$\hat{A}_2 = \begin{pmatrix} (1+A_2)/2 & (1-A_2)/2 & 0 & 0 \\ (1-A_2)/2 & (1+A_2)/2 & 0 & 0 \\ 0 & 0 & (1+A_2)/2 & (1-A_2)/2 \\ 0 & 0 & (1-A_2)/2 & (1+A_2)/2 \end{pmatrix}$$

3.1. Determination from 4-channel direct-beam spectra

We first record 4-channel direct-beam spectra under non-reflecting condition or under a non-magnetic reflectance one; these data provide $F_1(\lambda)$, $F_2(\lambda)$ and the product of $P_1(\lambda)$ and $A_2(\lambda)$. To determine the optical component efficiencies, we first analyze the direct beam intensities acquired for all four spin flipper states. Under the condition that the sample is non-magnetic and the beam is unreflected, the following symmetry in measured intensities holds: $I_0^{++} = I_0^{--}, I_0^{-+} = I_0^{+-}$.

The flipping ratio R_1, R_2, R_3 can be defined as follows. As the condition is satisfied in this case, we can transform equation (S3) to obtain the following expression:

$$R_1 = \frac{I_0(10)}{I_0(00)} = \frac{1-(2F_1-1)P_1A_2}{1+P_1A_2}$$

$$R_2 = \frac{I_0(01)}{I_0(00)} = \frac{1-(2F_2-1)P_1A_2}{1+P_1A_2} \quad \text{(S4)}$$

$$R_3 = \frac{I_0(11)}{I_0(00)} = \frac{1+(2F_1-1)(2F_2-1)P_1A_2}{1+P_1A_2}$$

This allows Equation (S4) to be reduced to a simplified form, enabling the evaluation of the flipping efficiencies F_2, F_2, and the combined polarizer–analyzer efficiency product P_1A_2. These values are derived from the measured 4-channel intensities $I(ij)$, as follows:

$$F_1 = \frac{R_1 + R_2 - R_3 - 1}{2(R_2 - 1)} = \frac{1}{2}\frac{I_0(11) - I_0(10) - I_0(01) + I_0(00)}{I_0(00) - I_0(01)}$$
$$F_2 = \frac{R_1 + R_2 - R_3 - 1}{2(R_1 - 1)} = \frac{1}{2}\frac{I_0(11) - I_0(10) - I_0(01) + I_0(00)}{I_0(00) - I_0(10)} \quad \text{(S5)}$$
$$P_1A_2 = \frac{(1 - R_1)(1 - R_2)}{R_3 - R_2R_1} = \frac{I_0(00)^2 - I_0(00)I_0(01) - I_0(00)I_0(10) + I_0(10)I_0(01)}{I_0(10)I_0(00) - I_0(01)I_0(10)}$$

3.2. Determination from 4-channel reflectance of a magnetically saturated sample

When performing polarized reflectivity measurements on a magnetically saturated sample, the spin-dependent reflectivities satisfy the following relationships: $R^{++} \neq R^{--}, R^{-+} = R^{+-}$. Under this condition, Equation (S5) can be extended to separately determine the polarization efficiencies of the polarizer and analyzer.

$$A_2 = P_1 \frac{(2F_1 - 1)\big(I(00) - I(01)\big) + I(10) - I(11)}{(2F_2 - 1)\big(I(00) - I(10)\big) + I(01) - I(11)} \quad \text{(S6)}$$

By substituting Equation (S5) into the previously derived expressions, we can isolate and evaluate the individual values of P_1 and A_2.

$$P_1 = \left[\frac{(1 - R_1)(1 - R_2)}{R_3 - R_2R_1}\frac{(2F_2 - 1)\big(I(00) - I(10)\big) + I(01) - I(11)}{(2F_1 - 1)\big(I(00) - I(01)\big) + I(10) - I(11)}\right]^{1/2}$$
$$A_2 = \left[\frac{(1 - R_1)(1 - R_2)}{R_3 - R_2R_1}\frac{(2F_1 - 1)\big(I(00) - I(01)\big) + I(10) - I(11)}{(2F_2 - 1)\big(I(00) - I(10)\big) + I(01) - I(11)}\right]^{1/2} \quad \text{(S7)}$$

The statistical uncertainties in the efficiencies were estimated by propagating the error bars associated with the measured intensities using error propagation.

References

1. Stewart, R. Oxford School on Neutron Scattering. In Proceedings of the Lecture notes of 12th Oxford School on Neutron Scattering; (2011).
2. Hiroi, K.; Shinohara, T.; Hayashida, H.; Parker, J.D.; Oikawa, K.; Harada, M.; Su, Y.; Kai, T. Magnetic Field Imaging of a Model Electric Motor Using Polarized Pulsed Neutrons at J-PARC/MLF. *J. Phys.: Conf. Ser.* ***862***, 012008 (2017), doi:10.1088/1742-6596/862/1/012008.
3. Shinohara, T.; Hiroi, K.; Su, Y.; Kai, T.; Nakatani, T.; Oikawa, K.; Segawa, M.; Hayashida, H.; Parker, J.D.; Matsumoto, Y.; et al. Polarization Analysis for Magnetic Field Imaging at RADEN in J-PARC/MLF. *J. Phys.: Conf. Ser.* ***862***, 012025 (2017), doi:10.1088/1742-6596/862/1/012025.
4. Wildes, A.R. The Polarizer-Analyzer Correction Problem in Neutron Polarization Analysis Experiments. *Review of Scientific Instruments* ***70***, 4241–4245 (1999), doi:10.1063/1.1150060.
5. Saerbeck, T.; Klose, F.; Le Brun, A.P.; Füzi, J.; Brule, A.; Nelson, A.; Holt, S.A.; James, M. Invited Article: Polarization "Down Under": The Polarized Time-of-Flight Neutron Reflectometer PLATYPUS. *Review of Scientific Instruments* ***83***, 081301 (2012), doi:10.1063/1.4738579.
6. Takeda, M. (JAEA) *Private Communication*. 2023

Disclaimer/Publisher's Note: The statements, opinions and data contained in all publications are solely those of the individual author(s) and contributor(s) and not of MDPI and/or the editor(s). MDPI and/or the editor(s) disclaim responsibility for any injury to people or property resulting from any ideas, methods, instructions or products referred to in the content.